International Conference on Space Optics—ICSO 2018

Chania, Greece

9–12 October 2018

Edited by Zoran Sodnik, Nikos Karafolas, and Bruno Cugny

Evaluation of straylight characteristics of the Sentinel-5 NIR spectrometer optics

M. Merschdorf

L. Platos

P. Petruck

B. Michel

et al.

International Conference on Space Optics — ICSO 2018, edited by Zoran Sodnik, Nikos Karafolas, Bruno Cugny, Proc. of SPIE Vol. 11180, 111802R · © 2018 ESA and CNES · CCC code: 0277-786X/18/$18 · doi: 10.1117/12.2536018

Evaluation of Straylight Characteristics of the Sentinel-5 NIR Spectrometer Optics

M. Merschdorf[a], L. Platos[a], P. Petruck*[a], B. Michel[b], B. Harand[b]
[a]Jena-Optronik GmbH, Otto-Eppenstein-Strasse 3, 07745 Jena, Germany;
[b]Hembach Photonik GmbH, Finkenstrasse 1-3, 91126 Rednitzhembach, Germany

ABSTRACT

Jena-Optronik GmbH is developing the Sentinel-5 NIR spectrometer optics operating in the spectral range from 685 nm to 773 nm. It is purely based on refractive optics and makes use of a grating as dispersive element and a prism for aberration correction. One of the design drivers for the optics design is straylight as small absorption effects in the atmosphere need to be detected. To minimize false light on the detector the straylight characteristics have been analyzed and optimized together with Hembach Photonik GmbH. Special attention needs to be paid to the dispersive nature of the optics as compared to a pure imaging system. Sources of ghosts and scattered light such as surface roughness, particle contamination and scattering at mechanical surfaces are quantified. Main contributors to straylight are identified and strategies for straylight reduction are discussed. Among others this comprises effective means to suppress out-of-band light.

Keywords: Sentinel-5, spectrometer optics, diffraction grating, scattering, straylight analysis, ghost light analysis

1. INTRODUCTION

The Sentinel-5 instrument is part of the European Commission Copernicus Programme for monitoring the earth[1]. It will be a payload on the MetOp-SG A-satellites which circulate the globe on a sun synchronous polar low earth orbit of about 800 km height. As such it will also assist the operational meteorological observations of the MetOp programme for the timeframe of 2020 to 2040. The instrument comprises five spectrometers covering spectral bands from the ultraviolet (UV) to short wavelength infrared (SWIR) wavelength range and can detect the presence and local distribution of various gases and aerosols in the earth atmosphere.

In the Sentinel-5 instrument, light from a common telescope (including a polarization scrambler) passes through a slit homogenizer. The slit image will be spectrally split using a dichroic beam-splitter into the UV-visual (VIS) and near-infrared (NIR) spectral bands and to the respective spectrometer optics. The purpose of the NIR spectrometer optics is to spectrally disperse and image the light leaving the entrance aperture (slit homogenizer) onto the detector.

Jena-Optronik GmbH is developing the NIR spectrometer optics operating in the spectral range from 685 nm to 773 nm. It is purely based on refractive optics and makes use of a grating as dispersive element and a prism for aberration correction. One of the design drivers for the optics design is straylight as small absorption effects in the atmosphere need to be detected. The false light analysis for dispersive optical systems differs from pure imaging systems. The dispersive elements will fan out the spectral components and out-of-band light will not travel along the nominal beam path to the detector which is normally well controlled by field and aperture stops. This necessitates careful design of the shielding. Further on, out-of-band light is not recorded by the detector and its scattering contributions can barely be mitigated in post processing. Limiting the out-of-band spectral range is therefore a key ingredient to minimization of straylight effects.

The goal of this study is to analyze the straylight which consists of different contributions:

Ghost light is caused by non-nominal (unwanted) specular reflections from opto-mechanical parts. Depending on the mechanism they are created, ghosts may produce a more or less unstructured background signal on the detector, thus reducing image contrast and therefore its dynamic range, unless it can be subtracted by calibration. However, ghosts can also lead to hot spots causing erroneous measurements. The latter is typically the case if the detector lies in or close to the focus of a ghost path or if there are pairs of plane surfaces interacting with one another (detector plane, prism surfaces, grating etc.). Once the light source is created, the simulation of ghosts is purely deterministic.

Light scattering, on the other hand, has typically a twofold impact on the image: a "halo" about the nominal light caused by scattering from optical components and a diffuse background caused by all scattering processes. Hot spots may happen, depending on the position of the scatterer inside the optical system.

2. MODEL SETUP AND ANALYSIS WORKFLOW

2.1 Model setup

The system geometry and optical properties are based on ZEMAX and CAD models which were subsequently imported into the used straylight software ASAP and carefully merged.

In the following paragraph the optical model is described. The Sentinel-5 NIR spectrometer optics starts with a slit homogenizer and ends with the detector in the nominal direction of light propagation. The slit homogenizer (SH) consists of two parallel, highly reflecting mirrors at a short distance from each other which form the slit. It is illuminated by the telescope (not part of the model). Multiple reflections from the mirror in the direction normal to the mirrors ("spectral direction") lead to a beam homogenization whereas in the direction along the slit ("spatial direction") no homogenization takes place. The homogenization thus induces an astigmatism into the beam, because rays appear to originate from the beam homogenizer entrance aperture, when viewed parallel to the slit direction, but rather from the exit aperture, when viewed in normal direction. The mechanical surrounding of the slit homogenizer consists of two plane surfaces which are tilted by 10 degrees to the optical axis and 20 degrees to each other. Subsequently, the beam passes through a dichroic beam splitter (BS) and the first collimator lens (COL1). After reflection from two fold-mirrors (FOLD1, FOLD2), light hits the second collimator lens (COL2) which also compensates for the astigmatism using a cylindrical surface, followed by the prism and grating which disperse the light spectrally and the camera lens group (CAM1 – CAM4) which finally images the light onto the detector (DET).

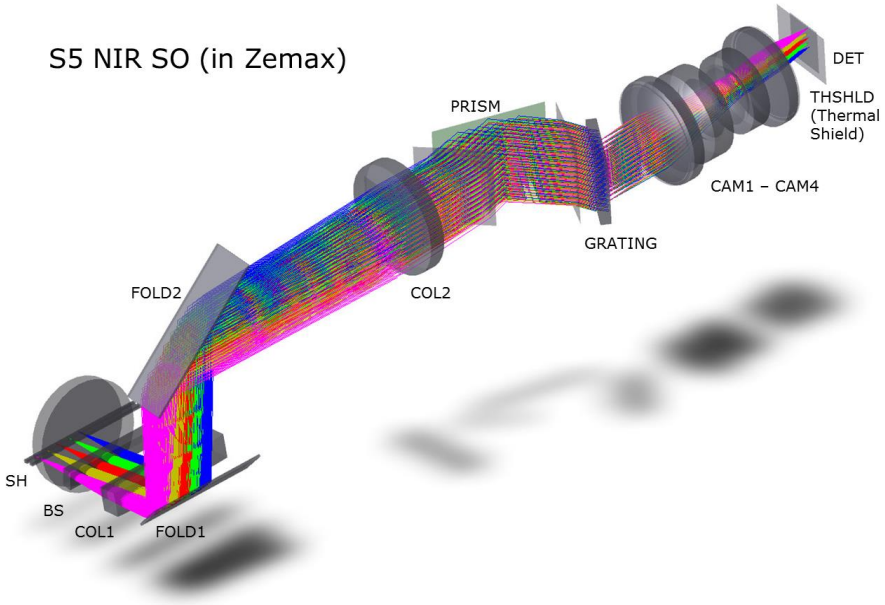

Figure 1: Sentinel-5 NIR spectrometer optics; optical system in ZEMAX including an exemplary ray trace

The mechanical model of the optical components was imported from CAD into ASAP. As opposed to the ZEMAX model, lens edges and chamfers are included, and will be regarded as polished surfaces except for chamfer at CAM3 front edge which is ground. The ZEMAX and CAD representation is then "merged", by replacing the optical surfaces of the CAD file with those from the Zemax file, and adjusting the bounds of the latter so that they exactly fit into the CAD model. The resulting "hybrid" ASAP model is shown in the next figure. For the ghost analysis, which was done first, this model – supplemented by models for beam homogenizer, detector, aperture stop and some additional straylight vanes from the Zemax file – is sufficient.

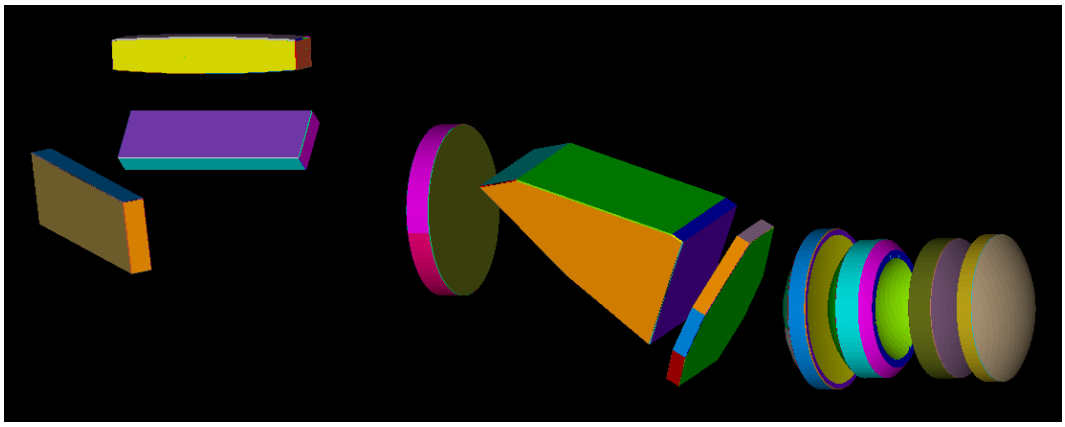

Figure 2: ASAP model of optical components, created by merging the ZEMAX with the CAD geometry (for ghost light analysis without any mechanical parts)

The CAD model is also used to complete the overall opto-mechanical system. For the scattered light analysis, the mechanical parts have to be imported into ASAP, too. Due to the level of detail in design this import has created around 22.000 objects in ASAP. This large number of objects would slow down simulations considerably. ASAP simplification of the outer geometry of the CAD model (which is not "seen" by the rays) was done to reduce the number of objects in ASAP to around 13.000 objects.

Dedicated coatings are assigned to all optical surfaces. The edges of the lenses are uncoated. Also a specular reflectivity needs to be assigned to the detector and the non-optical surfaces of the prism. For the analysis of the scattered light, scattering models have to be assigned to all relevant scattering objects. Only that part of scattered light is considered, that is relevant for the straylight performance of the system. This is achieved by using so-called important edges.

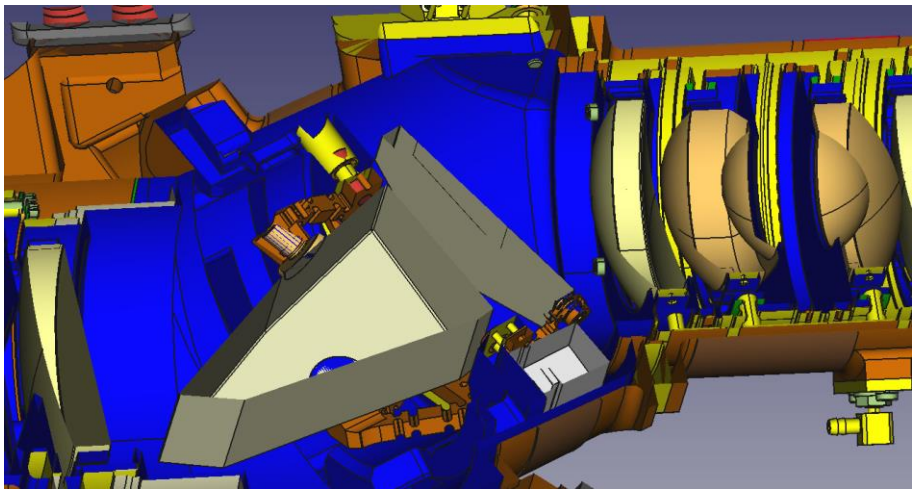

Figure 3: Sectional view through the reduced CAD model

The detector collects the rays passing the system on the nominal path as well as straylight generated inside the system. The detector was modeled as two rectangular planes. One plane (just in front of the other) has a reflectivity according to specifications. The second plane is the "real" detector used to collect light. In ASAP it is an absorbing, rectangular plane. Position and inclination are given by the ZEMAX model. The detector is covered by a thermal shield (THSHLD) with a window in front of the detector.

For analysis purposes it is useful to subdivide the detector into the different regions: from 685 nm to 710 nm (NIR1), from 745 nm to 755 nm (NIR2a), and from 755 nm to 773 nm (NIR2). To define these regions, a rectangular source in the exit of the slit homogenizer which is illuminating the complete aperture of the NIRSO is used. Its rays are traced to

the image plane for a selected set of wavelength. The slit image lines for the selected wavelengths mark the areas on the detector for relevant wavelength ranges called NIR1, NIR2 as well as NIR2a and the out-of-band lines near to the detector borders. For the analysis a test scene is assumed where one side of the (spatial) image is dark and the other bright, both with a given wavelength spectrum.

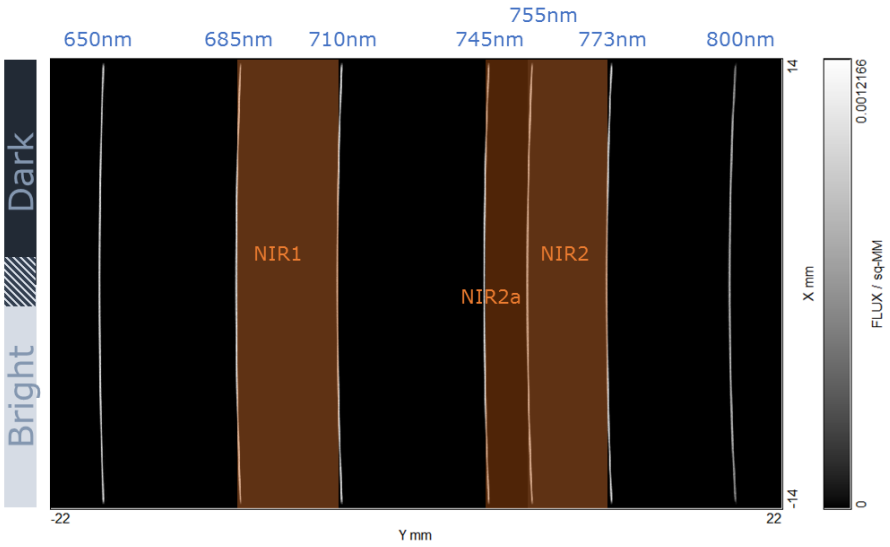

Figure 4: Slit images on the detector for different limiting wavelengths for definition of relevant wavelength ranges

The transmission grating splits the wavelengths into beams with different emergent angles. Due to the very small grating constant of 627 nm (distance between grating lines) and the angle of incidence of about 24 degrees, the number of diffraction orders for the considered wavelengths is low, i.e. only the -1st order of diffraction (nominal order) and the 0th order occur for the wavelength range between 650 nm and 800 nm. Higher orders may be generated for other angles of incidence and also for the lower wavelengths of the extended range.

ASAP has severe restrictions when modelling the diffraction from a grating. Although it can model the various diffraction order efficiencies, this can be done only in transmission, only in reflection or with transmission and reflection efficiencies proportional to each other. In other words, transmission and reflection efficiencies cannot be assigned independently. Also, the diffraction orders efficiencies are not wavelength dependent: only one set of coefficients is used per simulation. The real spectral dependence of grating must therefore be approximated by many wavelength range specific functions. Furthermore, to overcome the restrictions on grating reflection and transmission coefficients, an improved but rather complex model for the grating is implemented by using several sub-grating surfaces.

For modelling optical surface roughness an adapted three parameter Harvey scatter model is used. The optical surface roughness scattering takes place at every optical surface. For all surfaces a RMS roughness value of 1 nm was assumed. As the scatter model depends also on the refractive indices differences the scatter models vary for the optical surfaces. Forward scattering with small angles towards the nominal ray direction dominates in this type of scattering even more than for particle contamination scatter and was therefore simulated in the scatter angle range between 0 degree and 0.5 degrees separately and combined afterwards with simulation for scatter angles above 0.5 degrees.

For simulating particle contamination, the scatter models are Harvey fits to Mie scatter models. Fits were performed for 500 nm, 700 nm and 900 nm. For other wavelengths the model parameters are linearly interpolated between the fitted models. The final model is a weighted sum of four Harvey models each with three parameters. The particle contamination scattering takes place at every optical surface. For all surfaces a particle obscuration level of 50 ppm was assumed and therefore the scatter model is the same for all optical surfaces. Forward scattering with small angles towards the nominal ray dominates in this type of scattering and was simulated in the scatter angle range between 0 degree and 2 degrees separately and combined afterwards with simulation for scatter angles above 2 degrees.

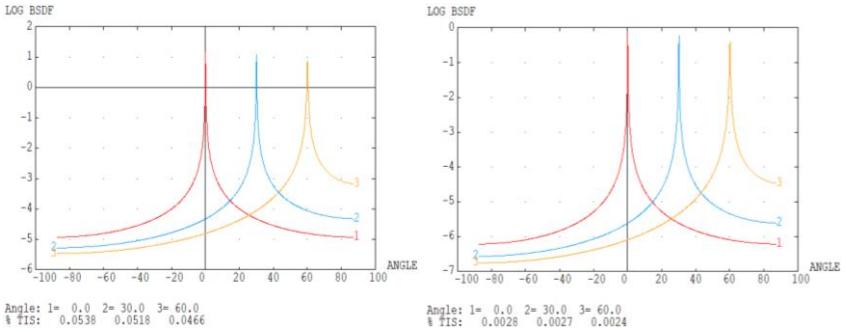

Figure 5: left: BSDF of fold mirrors; right: BSDF of optics made of SQ0; both at 730 nm wavelength

All non-optical/mechanical parts are assigned to one out of three different scatter models related to the coating chosen for each part: (1) Acktar Magic Black for all straylight critical mechanical surfaces, (2) a scatter model for bare metal parts or (3) a scatter model for glue pads used to fix optical elements. None of these models contains a wavelength dependence. The Acktar model was taken from in-plane BRDF measurements. The two other models are not based on measurements, but on plausible assumptions, taking into account a pronounced increase of the BRDF for grazing incidence. The angular variation of the BRDFs for different angles of incidence is shown in the figures below.

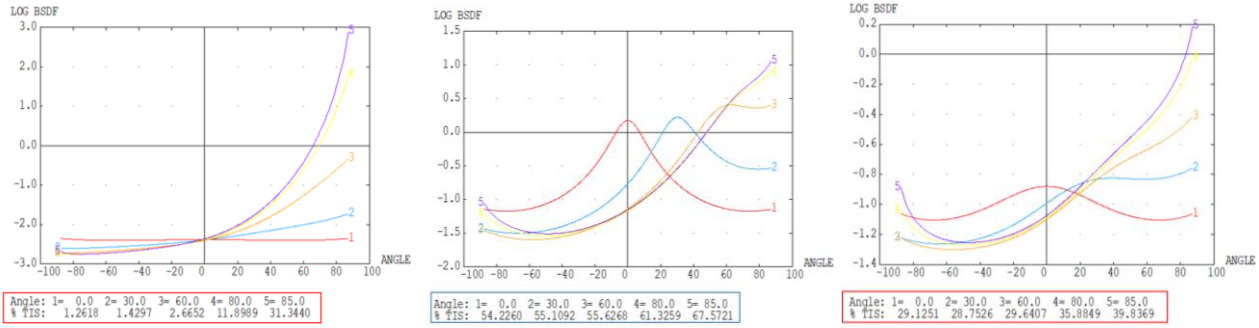

Figure 6: BRDF models; left: Acktar Magic Black; center: bare metal; right: glue pads

After system setup, two types of simulations are performed: qualitative simulations, focusing on the path analysis of selected paths, and a quantitative analysis that computes the detector irradiances of the nominal and ghost/scattered light. The latter is then used as input for the evaluation of specific straylight requirements which are not discussed in detail in this paper.

2.2 Straylight analysis implementation

The investigated straylight analysis considers

(1) Ghost light, which means: non-nominal light reaching the detector that is caused by reflections from optical surfaces, by specular reflections from the detector and the non-optical surfaces of the prims and by non-nominal diffraction orders of the grating. Reflections that do not change position at which the rays hit the detector (as compared to the nominal light) are not counted as ghosts, because they have no negative influence on the system performance.

(2) First order scattering from optical components caused by surface roughness and contamination

(3) First order scattering from mechanical parts, comprising parts like baffles, lens holders, tubes etc.

Combinations of scattering and reflection were only included for detector and grating reflection. All available diffraction orders of the grating were applied in all simulations. These straylight contributors were analyzed separately first, subsequently summed up and finally evaluated for full analysis. The goal of the present analysis is a detailed understanding of the straylight paths and an evaluation of the particular straylight levels.

Straylight can be further categorized as follows:

a. In-field straylight which is caused by light sources inside the field-of-view of the system, which often is the imaged object itself.

b. Out-of-field straylight coming from sources outside the field-of-view of the system. In the current system, the exit aperture of the slit homogenizer is the only light source which means that there is no out-of-field straylight.

c. In-band straylight is caused by light in the same spectral region in which the system is intended to operate.

d. Out-of-band straylight is produced by light outside the nominal spectral range of the spectrometer.

In the present system we have to analyze only in-field straylight which, however, consists both of in-band and out-of-band straylight. The light source producing the straylight is the imaged scene itself.

In the following, we consider as 'direct light' all light that is starting at the slit homogenizer within the nominal angle range and that reaches the detector on the nominal light path (i.e. transmission through lenses, reflections at fold mirrors, diffraction in -1st order in transmission at grating). Direct light within the nominal wavelength bands of NIR1 (685 nm – 710 nm) or NIR2/2a (745 nm – 773 nm) is called 'nominal light'. All other direct light is called 'direct out-of-band light'.

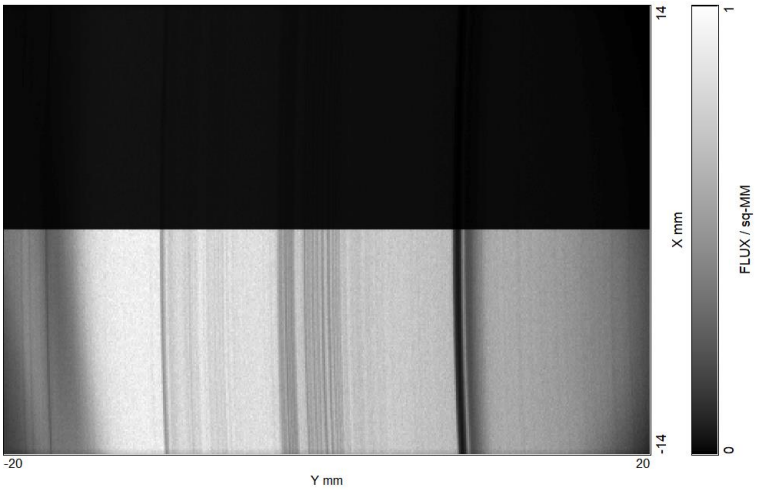

Figure 7: Direct light irradiance of the test scene including the specified input spectrum on the detector in linear scale; the irradiance is scaled to the maximum, thus the dark zone which is about 100 times darker appears as almost unstructured black

Straylight analysis normally starts with the computation of illuminated objects and critical objects, the latter being all opto-mechanical surfaces that can be "seen" from the detector.

Illuminated objects are determined by tracing rays from the slit light source into the system and collecting all absorbing objects that are hit by rays. These simulations were done for all wavelengths in 5 nm steps. In the simulations reflections at the grating, the detector and optical surfaces were allowed. Also all diffraction orders of the grating are considered. As the source angle is limited by the telescope aperture, only a few objects are hit by direct light. Most of the illuminated objects are hit by reflections at optical surfaces. At the end these simulations result in two lists of objects which are illuminated. One list contains all illuminated objects and the second list contains only those objects illuminated by direct light plus objects directly illuminated by the 0th diffraction order. The latter is needed as input for single scattering calculations, whereas the first is useful to estimate higher-order straylight.

Critical objects are determined by tracing rays from the detector into the system and collecting all absorbing objects that are hit by rays. Those objects are in the view of the detector. These simulations were done for all wavelengths in 5 nm steps where the detectors were used as light source with Lambertian scattering. For determination of objects near the detectors, which are normally most critical, the optical surface of CAM4 was set absorbing and the detectors were scattering into the hemisphere. For determination of all other objects that are critical, the optical surface of CAM4 was reset to its correct optical properties again and the detectors were scattering towards the aperture of optical surface of

CAM4. These simulations result in two lists of objects which are critical. One list contains all critical objects (including reflections) and the second list contains only critical objects which can be seen directly from the detector. Once again, the second list is relevant for single scattering calculations, whereas the first is only for information purposes.

Objects that are illuminated and critical objects at the same time are called “dangerous objects” and give rise to single-scatter contributions on the detector.. There are two options which can be possible to be dangerous objects. One is that objects that are illuminated directly and can be seen from the detector at the same time. The other one is that all objects that are illuminated directly and by reflections and at the same time can only be seen directly from the detector. Dangerous objects are able to scatter in first order the light towards the detector. All those objects are assigned to important edges. Finally, there is a list which contains all dangerous objects with the assignment of the correct scattering model and their correct important edges.

Finally, to remove statistical variations in simulation different possibilities of smoothing data were tested to get a more suitable representation of the data as we got by simple averaging. We decided to make a mix of interpolation of a polynomial curve in spatial direction and Fourier space low pass filtering in spectral direction.

3. STRAYLIGHT ANALYSIS RESULTS

In this chapter the results of the straylight analysis are presented. Each chapter starts with the straylight irradiance on the detector. This is followed by the distributions of the straylight normalized to the nominal light irradiance and the evaluation of the applicable requirements. Afterwards the straylight is analyzed by regarding the origin which is given by the optical paths analysis and discussion of noticeable features.

The irradiance distributions without normalization on the detector are shown as gray scale plots with adapted scaling ranges. The brightness relates to the irradiance value. These pictures are shown for (1) all wavelengths, (2) for in band wavelengths only and (3) for out of band wavelengths only. The gray scale range is equal for all three pictures.

For the quantitative analysis the irradiance distributions were evaluated regarding maximum irradiances as well as spectral and spatial variations. These results are all normalized to the nominal light irradiance and shown as profile curves with the x-axis representing a detector position. For better orientation we have marked the NIR1 & NIR2/2a range limits by dashed lines. The assigned measurement spectrum wavelengths are increasing from left to right. That means that NIR1 is on the left side and NIR2 is on the right side of the images and spectral profile plots.

3.1 Ghost light analysis

The analysis considers ghost straylight which means: non-nominal light reaching the detector that is caused by reflections from optical surfaces, by specular reflections from the detector, all surfaces of the prism, polished lens rims and chamfers and by all diffraction orders of the grating. The beam splitter in front of the spectrometer optics system is included in the calculations, too. Also considered was partial reflection at the grating stop and the thermal shield in front of the detector. The simulation was limited to second order ghosts except of an allowed third order process at the grating (for non-nominal diffraction orders). This means that a maximum of two reflections occurred at light-transmissive surfaces.

In general, the observed ghost patterns can be classified into three different types: standard, inverted and both. Standard type means that the bright side of the ghost pattern is on the bright side of the nominal light. In contrary, inverted ghosts seem to be flipped, i.e. the bright side of the ghost appears on the dark side of the nominal light. The inverted type is more critical because ghost signal is compared to low nominal signal and thus relative ghost light is comparably high.

On the first view we can recognize sharp ghost lines on the dark side of the detector, like the Littrow peak in the center of the image (detector-grating reflections) next to the NIR2a range. The beam splitter internal ghost makes a greater part of the visible ghost light and looks similar to the nominal light but with a slight blue shift. This makes out-of-band light shifting into the NIR1 and NIR2 areas marked by the dashed lines.

Following pictures show the irradiance distributions of ghosts on the detector.

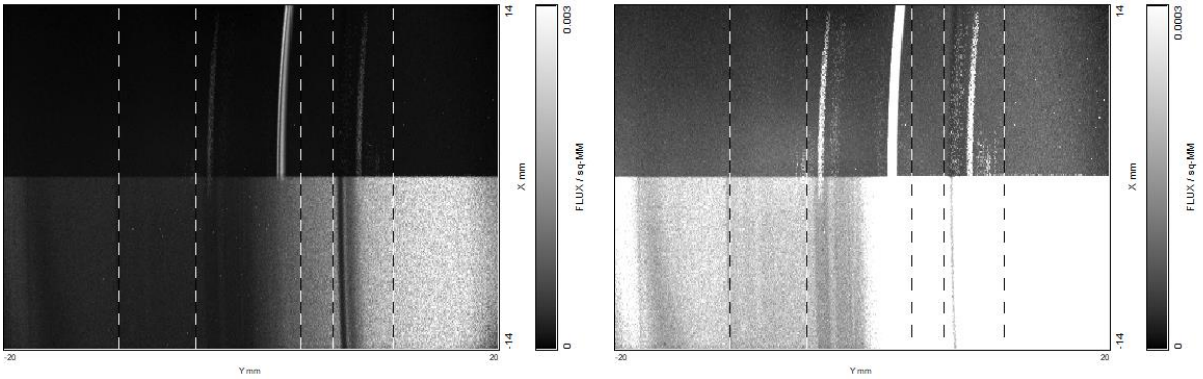

Figure 8: Ghost light irradiance on the detector (raw data) for all wavelength (520 nm – 930 nm); the left image is scaled for the bright slit side on the bottom; in the right image the scaling max was reduced by a factor of 10 to show the irradiance of the weaker ghosts on the dark side

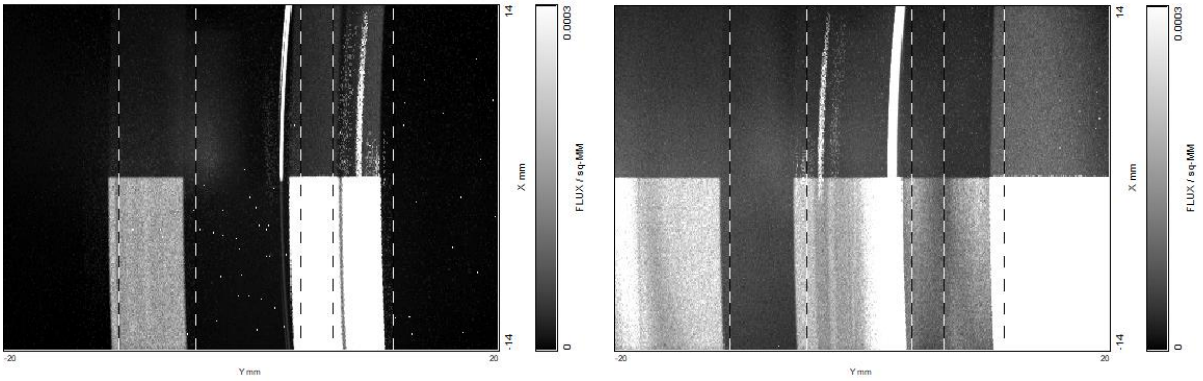

Figure 9: Ghost light irradiance on the detector (raw data) for in-band wavelength (left image) and out-of-band wavelength (right image)

Further details are shown in the paths analysis. The path analysis lists the ghost paths with the highest flux on the dark and bright in-field areas on the detector. The ghosts on the dark side are more important as the normalization to the nominal light makes the straylight level for the dark side much higher. But except for the beam splitter ghost the absolute flux values are similar on both sides of the detector. Almost all of the found ghost paths are within the beam envelope of the nominal light path and cannot be blocked.

In the following some ray trajectories are shown for the strongest ghost paths (left side) together with the ghost image (right side) calculated for a selected wavelength (including 1 nm bandwidth). Note, all irradiances are shown only for the upper part of the detector, i.e. the dark side of the nominal illumination, because this area is the important one.

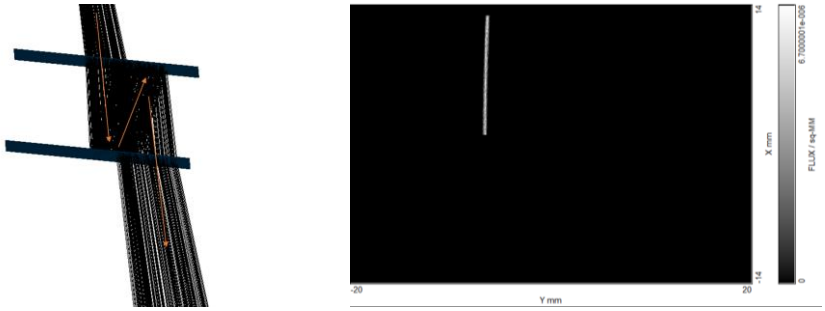

Figure 10: a prominent ghost is generated by reflections inside the beam splitter plate and is the strongest ghost of all. The reflections lead to a shift of the beam compared to the nominal beam and as a consequence the ghost image is slightly blue shifted (computed for wavelength 705 nm)

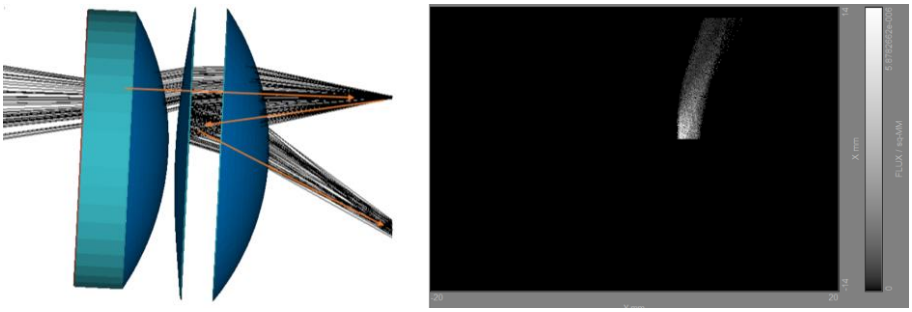

Figure 11: a ghost is generated by reflections at detector and the front surface of CAM4 lens; due to the curved surface of CAM4 the ghost image is spread and distorted and has a wavelength shift (computed for wavelength 645 nm)

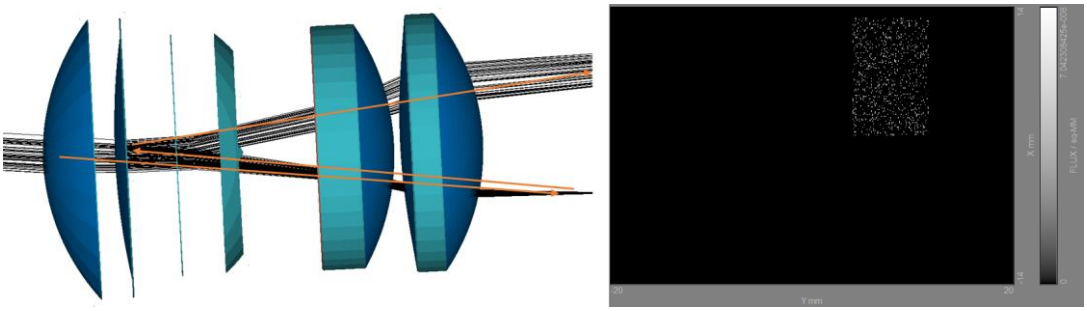

Figure 12: a ghost is generated by reflections at detector and CAM1 back surface (computed for wavelength 750 nm)

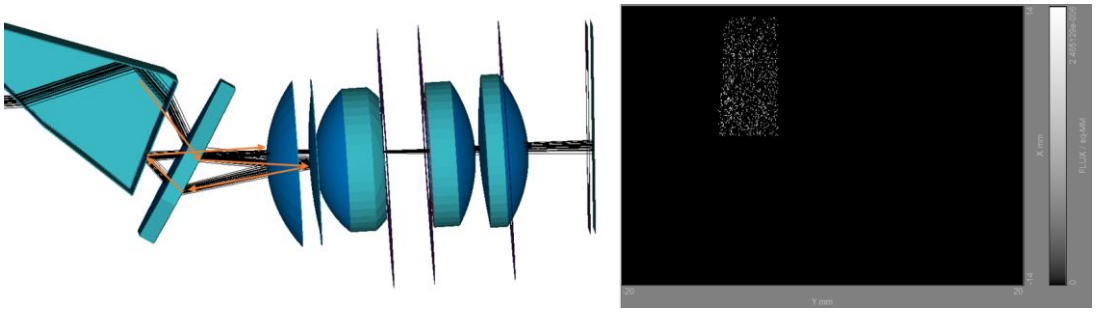

Figure 13: a more complex ghost is generated by a reflection from the back surface of the CAM1 lens; the light is then diffracted by the diffraction grating in nominal order and reflected back towards the detector by the prism's exit surface, passing through the grating again in 0^{th} order (computed for wavelength 615 nm)

All contributing surfaces except the beam splitter are coated with proper anti-reflection coatings. Most critical element is the beam splitter with a contribution of more than 25 % relative ghost flux. An adapted beam splitter design with spectral splitting on one side and broadband anti-reflection coating on the other side may improve this dominant ghost path.

Beside the beam splitter, both fold mirrors are key elements with respect to the generation of ghost light in the optical system, too. The preliminary design involved common metal coated mirrors with a broadband reflectivity. However, the beam splitter spectral characteristics as well as the input source spectrum are predefined by the customer. The effective wavelength range entering the spectrometer is significantly broader compared to the wavelength range of interest. Thus, out-of-band straylight can easily be generated for example by ghost light or its interaction with the grating. To overcome this issue the fold mirrors are introduced as bandpass filters, i.e. instead of single-layer metal coatings multi-layer dielectric mirror coatings are used. The reflectivity is adapted to the relevant wavelength spectrum and out-of-band spectral light shall be suppressed. However, the mirror substrates could then become a dominant source of ghost light because dielectric mirror coatings transmits out-of-band light. In order to suppress the transmitted light, the fold mirror substrates are made of absorbing material: neutral density filter NG5 by SCHOTT. An additional simulation specialized on these fold mirror ghosts were performed and it was found out that the ghost light irradiance on the detector is about ten orders of magnitude below the nominal light irradiance.

3.2 Scattering from particle contamination

The particle contamination scattering takes place at every optical surface. For all surfaces a particle obscuration level of 50 ppm was assumed and therefore the scatter model is the same for all optical surfaces. Forward scattering with small angles towards the nominal ray dominates in this type of scattering. For sake of getting a better ray statistics, it was simulated in the scatter angle range between 0 degree and 2 degrees separately and combined afterwards with simulation for scatter angles above 2 degrees. Statistical variations were removed by filtering in spatial and spectral direction, which can be applied well, as the straylight has only smooth structures.

The irradiance distribution looks like a strongly softened nominal light spectrum. The irradiance in the dark field rises towards the bright detector zone. Next to the exclusion zone (narrow zone in between bright and dark zone) the highest straylight levels can be expected.

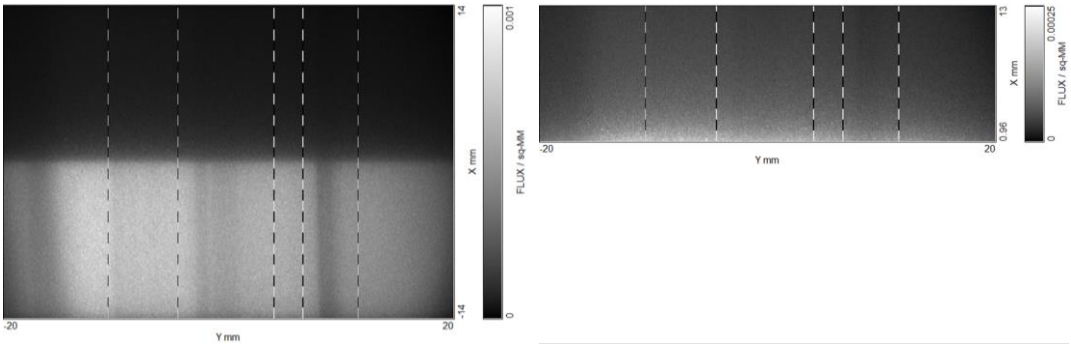

Figure 14: straylight irradiance by optical contamination on the detector (raw data) for all wavelength (520 nm – 930 nm); left: scaled for the bright slit side on the bottom; right: scaling max was reduced by a factor of 4 to show the irradiance of the weaker contributions on the dark side

The straylight by contamination scatter does not show remarkable structure. The contributing surfaces can be sorted by their distance from the detector due to losses by vignetting effects and spreading of straylight after the scatter process. The contributions vary only within one order of magnitude. In the first approximation, the first elements starting from the beam splitter up to the second fold mirror reveals slightly lower levels, while all other elements starting from the second collimator lens up to the detector show almost the same level with only minor variations.

Straylight by particle contamination depends (in first approximation) linearly from the contamination level. The assumed contamination level with 50 ppm is already very low and might be already challenging for some elements during the whole manufacturing, storage, assembly and test campaign. In order to further reduce straylight by particle contamination, theoretically the wavelength spectrum as well as the spatial frequency spectrum, i.e. solid angles of

illumination and detection per scattering surface, may are reduced. But within the design frame of the Sentinel-5 NIR spectrometer optics these options are justifiably discarded. Summarizing, straylight by particle contamination is not the biggest contributor but nevertheless the minimization of particle contamination is always targeted.

3.3 Scattering from optical surface roughness

The optical surface roughness scattering takes also place at every optical surface. Here, for all surfaces a RMS roughness value of 1 nm was assumed. As the scatter model depends also on the refractive indices differences the scatter models vary for the optical surfaces. Forward scattering with small angles towards the nominal ray dominates in this type of scattering even more than for particle contamination scatter and was therefore simulated in the scatter angle range between 0 degree and 0.5 degrees separately and combined afterwards with simulation for scatter angles above 0.5 degrees. Statistical variation were removed by filtering in spatial and spectral direction, which can be applied well, as the straylight has quite smooth structure.

The irradiance distribution looks like a softened nominal light spectrum. The irradiance in the dark field rises towards the bright detector zone, but not as strong as for particle contamination scattering, as the exclusion zone (narrow zone in between bright and dark zone) contains more of the scattered light from the bright side. Still the highest straylight levels can be expected next to the exclusion zone.

A paths analysis shows that the fold mirrors as well as the total reflecting surface of the prism are the strongest contributors. This was expected as the assigned scatter models for mirrors have the higher TIS values at the same level of roughness[2]. Except for this fact the contributing surfaces are sorted almost the same way like for scattering due to particle contamination. In general, transmitting substrate material with higher refractive index increases scattered flux.

Unsurprisingly, most effective approach to reduce straylight by surface roughness is to manufacture all optical surface as smooth as possible, especially reflective ones like mirrors. Nevertheless, in comparison to the other straylight contributors, surface roughness is of minor impact.

3.4 Scattering from mechanical parts

Subject of this section are non-optical parts that were found to be able to scatter light in first order towards the detector. That means that the light needs only one scatter process without lens reflections to reach the detector. There is an exception regarding additional reflections in the simulation: grating and detector are allowed to reflect as the reflectivity value of the detector is rather high and the diffraction in reflection of the grating can be high for some wavelengths and diffraction orders. This was considered in the determination of the important edges, too.

The irradiance distributions without normalization on the detector are shown as gray scale plots with adapted scaling ranges and for the dark side (as most relevant side) only. The gray level relates to the irradiance value. Following figures are shown for (1) all wavelengths, (2) for in band wavelengths only and (3) for out of band wavelengths only. The gray scale range is the same for all. For the quantitative analysis the irradiance distributions were evaluated regarding maximum irradiances as well as spectral and spatial variations.

Except for the lens edges (chamfers, circumferences etc.) and supporting surfaces (e.g. glue pads) most of the mountings and tubes are assigned the Acktar scatter model. Only few surfaces which cannot be coated (e.g. threads) are left blank and thus the ‘bare metal’ scatter model is used. Due to the characteristics of the Acktar model we mainly get rather smooth straylight distributions. On the other hand the statistical variation is quite big and needs stronger filtering. We found out that some high flux rays occurred and build some speckle-like structures even in the filtered data. Fortunately, the irradiance level is rather low, so that these results do not dominate the overall straylight on the detector.

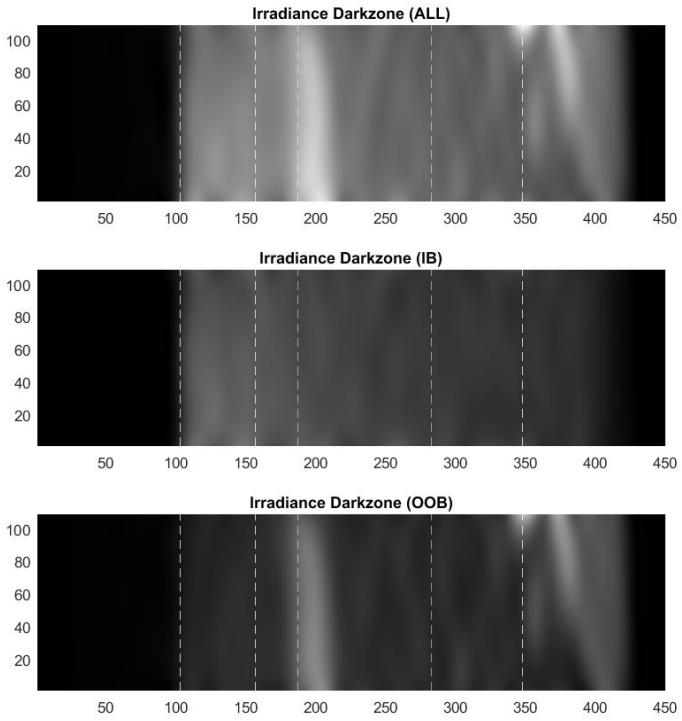

Figure 15: Straylight irradiance distribution on detector (dark zone only); top: all wavelengths (full spectrum); center: in-band wavelengths only; bottom: out-of-band wavelengths only; x-axis is reverse, i.e. longer wavelengths are on the left and shorter wavelengths are on the right; NIR1 (on the right) and NIR2/2a (on the left) bands are indicated by the dashed lines

Obviously the thermal shield mask in front of the detector limits the area that is illuminated by straylight. The shadow edge on the long wavelength end (on the left) is quite near to the NIR2 border. Despite the fact that scattered light on mechanical parts is rather low it is worth to have a look on the strongest straylight paths. In fact 97.1 % of the scattered light is derived from only seven scatter paths. Most of the light is scattered towards the detector at some lens holder baffle vanes after they are illuminated on the backside by detector reflections. In summation, more than 85 % of the scattered light is initially reflected by the detector. The wavelength ranges that appear in these paths are limited to the wavelengths (about 670 nm to 780 nm) that reach the detector on the nominal path for the initial reflection. Direct scatter also appears at some baffle vanes and uses other wavelengths ranges, too.

The following pictures show some exemplary rays to get an impression of the paths. As the rays are not running in the profile plane, but in 3D space and as they are only projected into this plane, the scattering locations may look to be at the wrong places, which is actually not true.

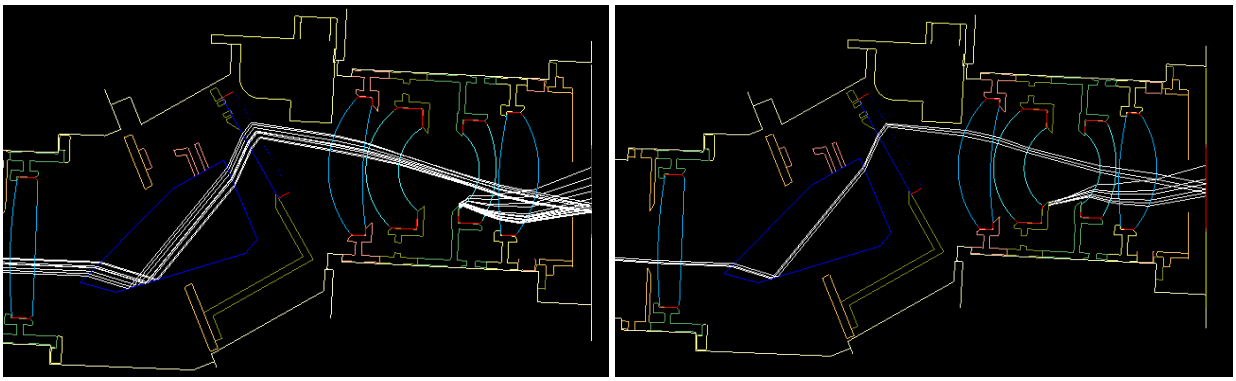

Figure 16: Prominent scattering paths; left: scattering at straylight vane of CAM3 lens; right: scattering at straylight vane of CAM2 lens; both after reflection at detector

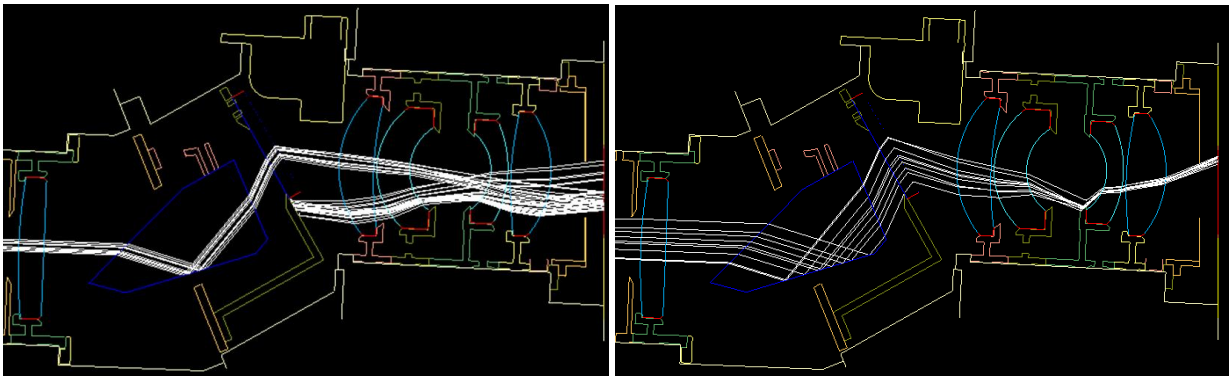

Figure 17: Prominent scattering paths; left: scattering at grating aperture mask after reflection at detector; right: scattering at edge of the straylight vane of CAM3 lens directly to the detector

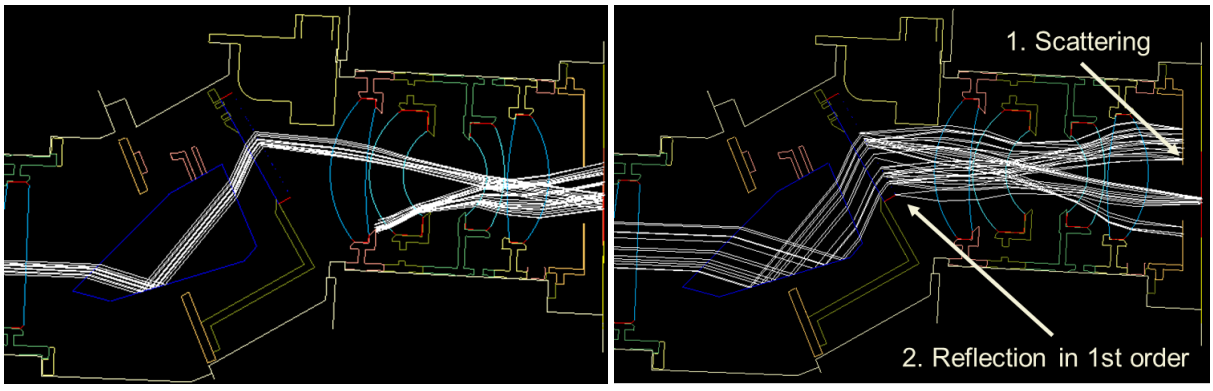

Figure 18 Prominent scattering paths; left: scattering at straylight vane of CAM1 lens after reflection at detector; right: scattering at thermal shield and reflection at grating in 1st order

In summary, most scattering paths are initially starting at the detector due to its comparably high reflectivity. In order to improve the overall straylight level due to mechanical scattering it seems worth to enhance the detectors behavior in terms of reflectivity. The secondary contributors are mainly identified by mechanical elements close to the detector and

close to the nominal beam envelope like the vanes in the CAM lens unit as well as the mountings of the grating and prism. In particular, the straylight vanes in the CAM unit are introduced to block rogue and ghost paths. Omission of these vanes is no option since even more critical paths will occur. Consequently, the use of high absorbing coatings (like from Acktar) is best choice. However, compared to the other straylight level contributors scattering by mechanical surface is not the dominant one.

4. CONCLUSION

In the present paper the optical and opto-mechanical design of the Sentinel-5 NIR spectrometer optics is introduced and the results of the straylight characterization and analysis are discussed.

In comparison of all relevant contributors like ghost light, scattering by particle contamination, scattering by optical surface roughness as well as scattering by mechanical surfaces, ghost light is most dominant and thus has the strongest impact. Here, the effect of some significant ghost paths is aggravated by inversion of the image so that the ghost signal of the bright side is compared with the nominal signal of the dark side. Most contributions to ghost light in the sensitive areas are generated by ghost paths using reflections from detector and the beam splitter internal reflections.

For improvement of ghost light we suggest to adapt the beam splitter design with spectral splitting on one side and broadband anti-reflection coating on the other side. Furthermore, a high-quality anti-reflection coating on the detector is highly recommended, too.

Scattered light is generated dominantly at optical surfaces, with particle contamination (calculated for 50 ppm per surface) having a larger contribution than surface roughness (calculated for 1 nm RMS per surface). However, the scattering distribution is very smooth and only minor out-of-band light is leaking into the in-band bands areas.

Regarding other options for improvement the presented design is almost state of the art in terms of cleanliness (particle contamination), surface polishing (roughness) and black coatings. One major improvement which we were able to implement was the use of the fold mirrors as spectral bandpass filters to reduce out-of-band light within the optical system. Therefore adapted coatings are used on highly absorbing mirror substrates made of NG5.

REFERENCES

[1] Irizar, J. et al., “Sentinel-5,” Proc. of International Conference on Space Optics (ICSO) 2018
[2] Dittmann, M. G., “Contamination scatter functions for stray-light analysis,” Proc. SPIE Vol. 4774, pp. 99, 2002